Accepted Manuscript

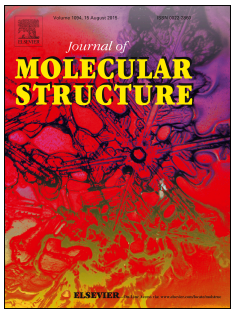

Synthesis, physicochemical and quantum chemical studies on a new organic NLO crystal: Cinnamoylproline

M. Venkateshan, J. Suresh

PII: S0022-2860(18)31504-7

DOI: https://doi.org/10.1016/j.molstruc.2018.12.071

Reference: MOLSTR 26008

To appear in: *Journal of Molecular Structure*

Received Date: 9 September 2018

Revised Date: 15 December 2018

Accepted Date: 18 December 2018

Please cite this article as: M. Venkateshan, J. Suresh, Synthesis, physicochemical and quantum chemical studies on a new organic NLO crystal: Cinnamoylproline, *Journal of Molecular Structure* (2019), doi: https://doi.org/10.1016/j.molstruc.2018.12.071.

Synthesis, Physicochemical and Quantum chemical studies on a new organic NLO crystal: Cinnamoylproline

M. Venkateshan*, J. Suresh

Department of Physics, The Madura College, Madurai – 625011, Tamilnadu, India.

Abstract:

Cinnamoylproline was synthesized and the crystal was grown from solution by the slow evaporation method. The crystal belongs to the trigonal crystal system with non-centrosymmetric space group $P3_1$. The calculated geometry and experimental geometry from single crystal X-ray data were compared. Intermolecular interactions were studied using Hirshfeld surface analysis and its real space functions were calculated using Atoms In Molecules (AIM) and its isosurfaces were visualized using Non-covalent interaction analysis. Optical transparency of the crystal was analyzed by UV-Vis analysis and it was found that the crystal has good optical transparency in the visible range and the lower cut-off wavelength was found to be 326 nm. In the photoluminescence spectrum, a broad emission peak at 369 nm was observed. The functional groups were analyzed using FTIR techniques and the vibrational frequencies from experimental and theoretical values were compared. It was inferred from the TG-DTA studies that the crystal was thermally stable up to 375°C. Kurtz-Perry powder SHG analysis was also carried out with KDP as a reference. It showed that the crystal has 1.08 times greater efficiency than KDP. The first hyperpolarizability tensor of the molecule was calculated theoretically and theoretical second order susceptibility was obtained and compared with the experimental susceptibility.

Keywords: Crystal growth, First hyperpolarizability, QTAIM, Hirshfeld surface analysis, Non Covalent Interaction (NCI), cinnamic acid.

***Corresponding author: (M. Venkateshan)**

Mobile: +91 9994344845

E-mail: m.venkateshan16@gmail.com

1. Introduction

Organic nonlinear optical (NLO) material are preferred over to the inorganic NLO material due to their higher order optical conversion efficiency. NLO materials find application in the fields of optical storage devices, terahertz wave generation, optical signal processing, frequency conversion, LASER remote sensing and medical diagnostics [1-6]. In organic single crystals, the organic molecules are packed or stabilized by intermolecular interactions like Van der Waals interactions and hydrogen bonding [7] which contribute significantly to the physical characteristics of the molecule. Hence a study of these interactions is important in our understanding of the NLO properties of these crystals. Hirshfeld surface [8-10] and its related 2D fingerprint plots [11] are simple tools that enable us to study and analyse these intermolecular interactions. Density functional theory (DFT) is helpful in estimating various molecular properties like equilibrium geometry, UV-Vis spectra, IR spectra, first order hyperpolarizability of NLO materials and the SHG susceptibility theoretically.

Cinnamic acid derivatives showed some medicinal properties like anti-cancer [12], anti-tuberculosis [13], anti-malarial [14], anti-fungal [15], anti-microbial [16], haemostatic agents [17] and also possess non-linear optical behaviour [18]. Likewise, some compounds containing proline showed NLO activity [19,20]. The amide derivatives of carboxylic acids can be prepared by treating with amino acids in the basic medium by the activation of carboxylic acid using carbodimides [21], $SOCl_2$ [22] or $POCl_3$ [23].

In the present work, single crystal of cinnamoylproline (CP) was grown by solvent evaporation technique and characterized by single crystal X-ray diffraction, Powder X-ray diffraction, UV-Visible spectra, FTIR spectra, Photoluminescence, TG-DTA and second

harmonic generation NLO studies. Also, DFT calculation was used in the molecular orbital analysis, UV-Vis absorption spectra, IR spectra, first order hyperpolarizability and second order nonlinear susceptibility calculation. The intermolecular interactions like C-H…O and O-H…O present in the crystal was studied using Hirshfeld surface analysis and 2D fingerprint plots. The topological analysis using Quantum Theory of Atoms In Molecules (QTAIM) [24] at the Bond Critical Point (BCP) was carried out to estimate its real space values to find hydrogen bond strengths. Non Covalent Interactions (NCI) [25,26] method has been used for visualizing the various types of interactions present in the crystal.

2. Experimental and theoretical methods

2.1 Synthesis

Cinnamoylproline was synthesized from the reaction of cinnamoyl chloride (98% purity) and proline (99% purity). Starting materials were purchased from Sigma Aldrich and Himedia. Cinnamoyl chloride (0.083 g) was dissolved in 5ml of THF (100mM) and 0.212 g of K_3PO_4 (200mM) was added and stirred for 1 hour. L-proline (0.058 g) was taken in 5ml of THF (100mM) and added to the above stirred mixture (Fig. 1). This reaction mixture was refluxed for 12 hours and then solvent was removed. To the precipitate, 20ml of water was then added and filtered. The insoluble material was filtered off. The filtrate was extracted with ethyl acetate. To the aqueous layer 2N HCl was added to get the pH of 2. After washing with water the solid product was the synthesized compound. (Yield : 78%).

2.2 Crystal growth

The synthesized compound was dissolved in methanol and stirred for 5 minutes to obtain a homogeneous solution. This solution was poured into a beaker and covered with perforated

polyethylene cover and kept in an undisturbed, dust free environment and allowed to evaporate slowly. After a few days colorless, hexagonal shaped crystals were formed.

2.3 Single crystal X-ray diffraction (SXRD)

A good quality optically clear 0.21 x 0.20 x 0.18 mm^3 sized crystal was mounted on the goniometer head of Bruker kappa APEX II diffractometer using the MoKα radiation source for X-ray data collection. The intensity data were collected at 20°C. Absorption correction for data was carried out using the SADABS program with multi-scan method. The structure was solved using SHELXS in direct method and refined least squares method using SHELXL embedded in SHELXTL-2014 [27,28]. Hydrogen atoms were fixed on the basis of riding model and refined isotropically and all other atoms were refined anisotropically. In final refinement cycles, the structure was refined as an inversion twin using TWIN/BASF commands with the BASF value of -0.13501. This yields the final, absolute structure parameter of (Flack [29] parameter x) -0.1 (15). Refined structure was validated using the software named PLATON [30] finally the CIF was validated using CheckCIF from IuCr. Thermal ellipsoid image and molecular packing diagrams were generated using ORTEP [31] and Mercury [32]. Intermolecular interactions were revealed from the PARST [33] program. Crystallographic data and refinement parameters were listed in Table 1.

2.4 Powder X-ray diffraction

Powder X-ray diffraction data were collected on Bruker ECO D8 powder diffractometer at room temperature using Cu Kα radiation with wavelength 1.5406Å. The 2θ scan range was 10-50°, with a step size of 0.02°.

2.5 Computational details

Theoretical DFT calculations for geometry optimization were done using the computational package ORCA 3.0.3 [34]. The experimentally obtained structure and optimized structure was overlaid and presented in Fig. S1. First hyperpolarizability tensor for the calculation of second order nonlinear susceptibility calculations was done using the software package Dalton [35,36]. The input file for ORCA to calculate geometry optimization was generated from experimental crystal data as initial coordinates with the DFT B3LYP level of theory with 6-311G(2d,2p) [37] basis set. This optimized geometry was used for finding UV-vis absorption wavelength, corresponding oscillator strength and IR vibrational frequencies. Non-linear properties like polarizability, hyper polarizabilities were calculated at the CAM-B3LYP [38] level of theory with NLO-V [39,40] as a basis set. NLO-V basis sets downloaded from the basis set exchange portal.

For the analysis of QTAIM and NCI, the Single Point energy calculation was done using the single crystal X-ray geometry as input. The molecules and its aggregates were selected in order to cover all the interactions (Fig. S2). The output wavefunction file was used for the analysis. For QTAIM analysis Multiwfn [41] software was used and for NCI study, NCIPLOT [42] program was used. The combined outputs were visualized using VMD [43] software.

3. Results and discussion

3.1 Single crystal X-ray diffraction studies

CP was crystallized in the trigonal crystal system with non-centrosymmetric space group $P3_1$. Its unit cell values are a = 15.9976(10) Å, b = 15.9976(10) Å, c = 13.4251(7) Å and V = 2975.5(4) $Å^3$. The asymmetric unit contains three crystallographically independent molecules of CP (say A, B, and C) (Fig. 2). The molecules A, B and C were overlaid and shown in Fig. S3. In all the three molecules the phenyl ring (C1-C6) is nearly a planar with the r.m.s deviation of 0.01

Å/0.0105 Å/0.006 Å for molecules A/B/C with the fitted atoms. The conformation angles χ^1 (N1-C13-C12-C11), χ^2 (C13-C12-C11-C10), χ^3 (C12-C11-C10-N1), χ^4 (C11-C10-N1-C13) and θ (C10-N1-C13-C12) of a pyrrolidine ring of A, B and C molecules are reported in Table 2. In all three molecules pyrrolidine ring (N1, C10-C13) adopts C_s-$C12^{\beta}$-exo conformation [44,45]. This is confirmed by Cremer-Pople puckering parameters (q_2, φ_2) [46] and the flap atom C12 from the mean plane drawn for another four atoms (Table 2). The atom C12 flap from the mean plane of N1, C10, C11, C13 for molecules A/B/C are 0.518(1) Å/0.558(1) Å/0.508(1) Å. The similar characters are observed in many analogous structures [45,47].

The pyrrolidine ring makes a dihedral angle of 32.10(2)°/30.92(2)°/36.31(2)° with the phenyl ring in A/B/C. The sum of the angle around N1 is 359.18 (2)°/359.71 (3)°/359.41 (2)° for A/B/C reveals that N1 is in sp^2 hybridization [48].

The crystal is stabilized through C – H … O and O – H … O interactions. In molecule A an intermolecular interaction O2A - H2A1 … O1A links symmetry related molecules forming a one dimensional chain motif C(7) (Fig. 3 (a)) with a base vector [001]. This similar pattern is followed in molecules B and C. Molecule A interconnects B through C2A – H2A … O3B, molecule B links C through the interaction C8B – H8B … O3C and C connects to A through the intermolecular interaction C1C – H1C … O3A. These C – H … O interactions form a three dimensional network (Fig. 3 (b)). The possible intermolecular interactions produced from PARST were listed in Table 3. C – H … π interactions are also observed. Since they are so weak so that they have omitted from the discussion.

3.2 Powder X-ray diffraction (PXRD) analysis

Powdered sample of as grown crystal was subjected to PXRD analysis to identify the crystallanity also to confirm that the crystal structures represent the bulk material in truth. PXRD

pattern was simulated and the peaks were indexed using Mercury software from experimental SXRD data. Fig. 4 represents the correlated spectrum of experimental and simulated PXRD patterns. The two spectra were matched well, which proves the synthesized bulk material is same as the single crystal and the well-defined peaks defines the crystallanity.

3.3 Hirshfeld surface analysis

SXRD data reveal the presence of intermolecular interactions present in the crystal structure. To study, the percentage of contribution of different intermolecular interactions present in the structure, Hirshfeld surface (HS) analysis was carried out. HS [9,49] along with 2D fingerprint plots [8,11] are interesting tools for visualizing and studying about intermolecular interactions. In order to construct HS and its associated 2D fingerprint plots the software called Crystal Explorer 3.1 [50] was used. 3D HS with the surface property of d_{norm} is an easy visualization tool generated from d_i, d_e and van der Walls radii. The d_{norm} is the ratio between the distance of the point from the surface to the interior atom (d_i) and the exterior atom (d_e) to the van der Walls radii (r^{vdw}). If the distance of an atom from the surface is lower than the van der Walls radii, then the d_{norm} will be negative shows that closer proximity indicates an interaction. This is specified as red spots. If the distance of an atom from the surface is higher than the van der Walls radii, then the d_{norm} will be positive shows that there is no possible interaction. This is specified as blue spots. The 2D fingerprint plot is another view of interaction, plotted from d_i vs d_e.

In order to find out whether all the three molecules have equal proportions of interactions, HS study was carried out for those molecules independently. The results were shown in Fig 5. It was inferred from the analysis in all respects that, all the molecules have equal

contributions to the crystal packing. Therefore molecule B was arbitrarily chosen for further analysis.

Fig. S4 shows the 3D d_{norm} surface generated with a surface area of 292.86 $Å^2$ and volume of 324.41 $Å^3$. The globularity (G) [51] (defines how much the structure varies from sphere (G = 1) of similar volume) value is 0.780 and the asphericity (Ω) [52] (defines the anisotropy of the structure) value is 0.295 suggests that the structure is nearly an oblate (for oblate Ω = 0.25) [52]. In this figure, there are two bright red spots corresponds to O - H…O interaction and one light red spot appearing corresponds to C – H…O interaction. For the O – H … O interactions the sum of distances d_i and d_e is 1.81 Å which is very much smaller than the van der Waals radii of 2.61 Å [53,54] indicate a bright red spot, and for C – H …O interaction d_i + d_e is 2.41 Å which is smaller than the van der Waals radii of 2.61 Å indicate a light red spot on the surface. 3D HS was translated to 2D fingerprint plots and they are presented in Fig. 5. In the FP plot O…H/H…C interaction shows two distinct sharp spikes [55]. The fingerprint analysis does not show the equal contribution of O … H and H … O interactions. O … H interactions are depicted as a sharp spike on the bottom left area and H … O interactions are presented as a sharp spike on the bottom right of fingerprint plot. O … H interactions contribute slightly higher (13.9%) than the H … O interactions (12.5%) (See supplementary data Fig. S5). C … H interactions were plotted as a pair of wings shaped [56], in this C … H interaction contributes (13.9%) higher than the H … C interaction (11.2%) (See supplementary data Fig. S6). These contributions may be arrising from the presence of weak C – H … π interactions and van der Walls interactions. Fig. S7 shows the individual contributions of interactions from HS analysis.

3.4 QTAIM and NCI

Bader's QTAIM theory was used to quantify the interaction energies present in the structure. The interaction energy is directly related to the electron density (ρ) at the BCP between the two atoms. In order to be a non-covalent interaction like hydrogen bonds, van der Walls interactions; the derivative of electron density called Laplacian of the electron density ($\nabla^2\rho$) should be positive. This Laplacian is further divided into three Eigenvalues (λ_1, λ_2 and λ_3). The NCI index uses the sign of the λ_2 in order to differentiate attractive or repulsive interactions. The positive sign of λ_2 represent the repulsive steric crowding, the negative sign of λ_2 represent the attractive hydrogen bonds and the value near to zero corresponds to a van der Walls interaction. The NCI index also uses another derivative of density called reduced density gradient (S) which has a value nearer to zero at the BCPs. A graph plotting with sign(λ_2)ρ versus S is very helpful in understanding the type of interactions present in the structure. The NCI isosurface is red-green-blue colour coded based on the sign(λ_2)ρ value. Red represents repulsion, green for van der Walls interaction and blue represents strong hydrogen bonds [25,35].

QTAIM descriptors like electron density (ρ), Laplacian of the electron density ($\nabla^2\rho$), potential energy density (V), Lagrangian kinetic energy (G) at the BCP's were represented in the Table 4. The hydrogen bond energies were calculated using the relation E_{HB} = V(r)/2. According to Popelier [57] for a hydrogen bond ρ must fall in the range 0.002 to 0.035 a.u and $\nabla^2\rho$ value in between the range 0.024 to 0.139 a.u.

Results obtained from the topological analysis of the selected bonds from PARST program are tabulated in Table 4. From this table the estimated ρ value ranges from 0.00221 to 0.02894 a.u. and $\nabla^2\rho$ value ranges from 0.0118 to 0.11025 a.u. The Laplacian values of some C-H…O bonds are well below from the required value and these bonds have very minimum interaction energies. These can be ratified from the SXRD data of bond lengths and bond angles

of these bonds (Table 3). So these interactions may be considered as van der Walls interactions. Therefore, we have only considered the first seven hydrogen bond interactions in Table 4, which obeys the value given by Popelier.

In the title compound O-H…O interactions plays the major role for molecular packing by giving the moderately strong interactions as expected. This can be supported by the NCI plot with a light blue isosurface surrounds a QTAIM BCP in between the O-H…O bond and well separated broad blue spike in the 2D reduced density gradient graph (Fig. 6). The energy values are in the range -31.81 to -30.027 kJ.mol^{-1}. These values are in good agreement with the previously reported O – H … O energy values. Chahkandi [58] and co-workers analyzed the O – H …O and C – H … O interactions of 4-[(4-chlorophenyl)amino]-4-oxobutanoic acid and reported its interaction energies. For O – H … O interaction they have reported energies of -50.08 and -44.61 kJ.mol^{-1} in D…A distance of 2.625 Å and 2.946 Å. In the title compound we have found energies corresponding to O – H … O interactions as -31.81, -30.608 and -30.027 kJ.mol^{-1} with D…A distance of 3.333, 3.355 and 3.403 Å respectively (Table 3 and 4).

Further C – H …O analysis was done and obtained energies were lying between -8.027 to -7.581 kJ.mol^{-1}. The existence of these interactions was also identified by the formation of corresponding BCPs from QTAIM analysis and ratified from the NCI plot by an isosurface enclosed that BCP. These values are also concurred with the already existing C – H … O bond energies [59]. In comparison with the reported values, our values match adequately with the support of experimental SXRD bond lengths and bond angles. The smaller interaction energies were already assigned to van der Walls interactions are also present in the NCI plot isosurface and 2D reduced gradient graph.

3.5 HOMO - LUMO analysis

The studies on frontier molecular orbital expose the chemical reactivity, chemical hardness or softness of the molecule and kinetic stability [56]. The energy of HOMO (Highest Occupied Molecular Orbital) level is -6.642 eV and for LUMO (Lowest Unoccupied Molecular Orbital) level energy is -2.178 eV. The 3D plots of frontier molecular orbitals and energies of the HOMO, HOMO-1, HOMO-2, HOMO-3, HOMO-4, HOMO-5, HOMO-6, LUMO and LUMO+1 of CP computed at the B3LYP/6-311G(2d,2p) level are shown in Fig. 7. The positive phase is denoted as blue and negative phase is red. The HOMO level has the electron releasing capability and LUMO has the electron withdrawing capability. The energy gap between these levels is 4.464 eV. This energy gap is an important parameter to determine some of the molecular properties like chemical hardness (η), electronegativity (χ), electronic chemical potential (μ) and global electrophilicity index (ω).

HOMO level of energy is assigned as the ionization potential (I) and LUMO is assigned as electron affinity (A), $I = -E_{HOMO}$ and $A = -E_{LUMO}$. The electronegativity (χ) of a compound which measures the ability of attracting electrons towards its side can be calculated using the relation, $\chi = \frac{(I+A)}{2}$. From this relation electronegativity of CP is χ = 4.41 eV. Chemical potential (μ) can be described as the escaping capacity of electrons from its equilibrium state [60], it can be calculated using, $\mu = -\frac{(I+A)}{2}$. By using this chemical potential of CP is μ= -4.41 eV. The chemical hardness or softness tells about the reactivity, stability of a molecule. It can be obtained using the relations, $\eta = \frac{(I-A)}{2}, S = \frac{1}{2\eta}$. Using these relations, η = 2.232 eV, S = 0.224 eV^{-1}. This indicates that CP possesses high chemical stability. The global electrophilicity index (ω) is defined as $\omega = \frac{\mu^2}{2\eta}$. This defines the electron accepting ability or power of a molecule from the

surrounding without changing its stability [56]. The global electrophilicity index (ω) of CP is found to be ω = 4.356 eV.

3.6 UV-Vis analysis

Optical transparency and cut-off wavelength are necessary properties of a material to be acting as a NLO material [61]. The UV- Vis analysis was carried out in the wavelength range between 200 - 800 nm. The correlated theoretical and observed electronic spectra were shown in Fig. 8. Experimental and calculated electronic absorption wavelength, Excitation energy (E), Oscillator strength (f), orbital contribution calculated at B3LYP/6-311G(2d,2p) level were shown in Table S1.The calculated spectra obtained in gas phase consists of five absorption peaks centered at 210 nm, 219 nm, 244 nm, 270 nm and 292 nm. In the observed spectra the absorption peaks were found at 206 nm, 218 nm, 248 nm, 276 nm and 284 nm. The absorptions at 206 nm, 218 nm, 248 nm and 276 nm were corresponded to $\pi \rightarrow \pi^*$ transition, 284 nm attributed due to the transition $n \rightarrow \pi^*$ [62]. The CP has a lower cut-off wavelength at 326 nm and shows transmission in the entire visible region which makes it a potential material for NLO applications.

3.7 Photoluminescence

Photoluminescence (PL) is a process of spontaneous emission of light radiation when excited by an excitation light of a particular wavelength. The molecule with conjugated π bonds may exhibit PL activity. The PL emission spectra of CP was recorded in the range 320 to 500 nm at an excitation wavelength of 326 nm. The maximum emission was occurring at 369 nm which is in the UV region (Fig. 9). The PL spectra shows a broad emission, which supports the presence the strong intermolecular interactions.

3.8 FTIR analysis

The presence of functional groups of CP was analyzed from FTIR spectra and it was compared with the theoretical values calculated from DFT methods and a comparison was tabulated in Table 5 and pictured in Fig. 10. There are 91 normal modes of vibrations with no imaginary frequency were identified from theoretical calculations. There is some mismatch in frequencies arose due to the fact that the DFT calculation was carried out for geometry optimized structure in gas phase whereas the experimental frequencies were observed in solid crystal.

In the FTIR spectrum the peak at 3599 (3591) cm^{-1} is assigned to the O-H stretching of COOH group. The vibrations corresponding to C-H stretching of phenyl ring and pyrrolidine ring are observed at 3194 (3197) cm^{-1} and 3099 (3097) cm^{-1} respectively. The observed peak at 1736 (1745) cm^{-1} is assigned to C=O anti-symmetric stretching of carboxylic acid group. C=C skeletal vibration is observed at 1647 (1683) cm^{-1}. The vibration at 1571 (1587) cm^{-1} is assigned to C=O stretching. Aromatic C-C stretching is observed at 1446 (1497) cm^{-1}. The vibration peak at 1323 (1336) cm^{-1} is due to C-H in-plane deformation. The peaks at 1255 (1249) cm^{-1} and 1193 (1199) cm^{-1} are due to C-N stretching. The band at 977 (983) cm^{-1} is attributed to C-H out of plane deformation. The aromatic C-H wagging occurs at 902 (902) cm^{-1}. The vibration at 767 (757) cm^{-1} is due to C-H out of plane bending. C-H bending mode of vibration occurs at 653 (651) cm^{-1}. The values in the parenthesis indicate the theoretical wavenumber.

3.9 Thermal studies

Thermal stability is an important property for a potential NLO material. To analyze the thermal stability and to confirm the melting point of the material, the Thermo Gravimetric Analysis (TGA) and Differential Thermal Analysis (DTA) were carried out using a Perkin Elmer thermal analyzer from room temperature to 730°C at a heating rate of 20°C/min in the air. The results were depicted in Fig. 11. The crystal undergoes three steps degradation. Below 100°C

there is no significant weight loss was observed, hence, there is no solvent molecule was included into the crystal. In the DTA there is a sharp endothermic peak at 375.7°C; this is assigned to the melting point of the material. This shows that CP is suitable for high energy laser applications. The first weight loss of 4.5 % was observed at 303°C. The second stage degradation occurred between 305°C to 420°C, third stage between 420°C to 504°C. The second and third stage degradations are due to the evolution of some volatile compounds.

3.10 NLO SHG analysis

The second harmonic generation efficiency of powdered CP was analyzed using Kurtz and Perry powder technique [63]. A Q-switched Nd:YAG laser of wavelength 1064 nm was used as a radiation source. CP was uniformly grounded with the same particle size as that of KDP, which was used as a reference for SHG measurements. The SHG property of CP was confirmed from the emission of green wavelength (532 nm). Comparison of SHG efficiency of CP with KDP is depicted in Fig. 12. From the figure it can be concluded that SHG efficiency of CP is 1.08 times to that of KDP.

The quantum chemical approach is an easy and effective way of predicting NLO properties from the molecular electronic structure [64]. In order to calculate the SHG efficiency, polarizability and first order hyperpolarizability must be calculated. The polarizability and first order hyperpolarizability are the measure of an ability of an electric field to distort the electronic distribution of a molecule.

The total static dipole moment (μ), the mean polarizability (α), the anisotropy polarizability (Δα) and first hyperpolarizability (β) using the components x, y, z can be calculated using the relations given below.

Total static dipole moment, $\mu = \sqrt{\mu_x^2 + \mu_y^2 + \mu_z^2}$

The mean polarizability, $\alpha = \frac{\alpha_{xx}+\alpha_{yy}+\alpha_{zz}}{3}$

The anisotropy of polarizability is,

$$\Delta\alpha = \frac{1}{\sqrt{2}}\sqrt{(\alpha_{xx}-\alpha_{yy})^2 + (\alpha_{yy}-\alpha_{zz})^2 + (\alpha_{zz}-\alpha_{xx})^2 + 6\alpha_{xx}^2}$$

The First order hyperpolarizability equation is,

$$\beta = \sqrt{(\beta_{xxx}+\beta_{xyy}+\beta_{xzz})^2 + (\beta_{yyy}+\beta_{xxy}+\beta_{yzz})^2 + (\beta_{zzz}+\beta_{xxz}+\beta_{yyz})^2}$$

The outputs from Dalton software are reported in atomic units (a.u). Therefore, the calculated values have been converted into electrostatic units (esu) (α: 1 a.u. = 0.1482 x10^{-24}esu; β: 1 a.u. = 8.641 x 10^{-33} cm^5 esu^{-1}). The calculated values of μ, α, Δα and β for the compound were found to be 7.54759 D, 82.621 x10^{-24}esu, 71.9583 x 10^{-24}esu, and 3.307 x 10^{-30} cm^5 esu^{-1} respectively. The non-zero value of dipole moment indicates that CP is a polar compound. The values of the dipole moment, polarizability and first hyperpolarizability components were listed in Table 6. From the calculated β value it is possible to calculate the second order susceptibility $\chi^{(2)}$. The SHG susceptibility of a bulk material can be obtained using the relation [65],

$$\chi^{(2)}_{abc}(-2\omega;\omega,\omega) = NL\beta_{abc}(-2\omega;\omega,\omega)$$

Where, $N = 1/V_{cell}$ (V_{cell} is the unit cell volume). L is the local field correction factor. $L = f_a^{2\omega} f_b^{\omega} f_c^{\omega}$ and $f_a^{2\omega} = \frac{n_\omega^2+2}{3} = \frac{3}{(3-4\pi N\alpha_\omega)}$.Here n_ω is the refractive index and α_ω is the first order polarizability. The value of L was calculated with the approximation of $\alpha_{2\omega} = \alpha_\omega$ [66].

The experimental value of $\chi^{(2)}$(exp)can be calculated with $\chi^{(2)}(exp) = b \times \chi^{(2)}(KDP)$. Where, $\chi^{(2)}(KDP) = 2d_{36}$, b is the NLO efficiency compared with KDP (for CP the value of b is 1.08). The selected valued_{36} of KDP is the average value 1.6 x 10^{-9}esu. The second order susceptibility of CP was obtained as, $\chi^{(2)}$(cal) = 1.2506 x 10^{-9}esu and $\chi^{(2)}$(exp) = 3.456 x 10^{-9}esu.

4 Conclusions

The optically transparent NLO material CP was synthesized and grown from slow evaporation technique. PXRD revealed the crystallanity. From the comparison of PXRD diffractograms the phase purity was confirmed. FTIR and SXRD studies confirmed the structure of CP. Also SXRD revealed the non-centrosymmetric nature of CP. SXRD exposed the presence of O – H … O and C – H … O intermolecular interactions, which were further confirmed by Hirshfeld surface analysis of 3D surface and 2D finger print plots. Also interaction energies were quantified by QTAIM and its isosurfaces were visualized through colour coded NCIPLOT. UV-Vis analysis revealed the lower cut-off wavelength as 326 nm and also the existence of $\pi \rightarrow \pi^*$ and $n \rightarrow \pi^*$ transitions. Also, it revealed the transparency of the CP in the entire visible range. The broad emission of CP around 369 nm proven by PL with an excitation wavelength of 326 nm suggested that the CP can be used to design a UV laser. Thermal stability of the material was analyzed by TG-DTA which showed that the CP has a thermal stability up to 375°C. Also, it exposed the nature of three step degradation of CP. Kurtz-Perry powder method revealed the presence of SHG with an efficiency of 1.08 times greater than KDP. Theoretical calculations were performed for UV-vis absorption analysis, FTIR vibrational frequencies, HOMO-LUMO molecular orbital analysis and NLO SHG susceptibility. HOMO-LUMO analysis revealed the band gap of CP as 4.464 eV. From the HOMO-LUMO values, varies molecular properties related to its chemical stability were calculated. Theoretical first hyperpolarizability of CP was found to be 3.307 x 10^{-30} cm^5 esu^{-1} and the experimental and theoretical second order susceptibility values were obtained as 1.2506 x 10^{-9}esu and 3.456 x 10^{-9}esu respectively.

5 Supplementary crystallographic data

CCDC 1832360 contains the supplementary crystallographic data for this paper. The data can be obtained free of charge from The Cambridge Crystallographic Data Centre via www.ccdc.cam.ac.uk/structures.

Acknowledgements

The authors thank the management of The Madura College for their support, SAIF, IIT madras, Chennai for SXRD data collection, also SAIF, Cochin for TG-DTA analysis. The authors also thank Kalasalingam Academy of Research and Education for Powder XRD measurement. They also thank Department of chemistry, The Madura College for UV and FTIR support, Department of chemistry, V.H.N.S.N college, Virudhunagar for PL studies. MV thank Dr. Gajanan G. Muley, Asst. Prof., Sant Gadge Baba University, Amravati, for NLO studies.

References:

1) G. Peramaiyan, P. Pandi, N. Vijayan, G. Bhagavannarayana and R. Mohan Kumar, Crystal growth, structural, thermal, optical and laser damage threshold studies of 8-hydroxyquinolinium hydrogen maleate single crystals, *J. Cryst. Growth.*, 375 (2013) 6–9.
2) V. Kannan, K. Thirupugalmani and S. Brahadeeswaran, Studies on vibrational, NMR spectra and quantum chemical calculations of N-Succinopyridine: An organic nonlinear optical material, *J.Mol. Struct.*, 1049 (2013) 268–279.
3) T. Pal, T. Kar, G. Bocelli and L. Rigi, Synthesis, Growth, and Characterization of L-Arginine Acetate Crystal: A Potential NLO Material, *Cryst. Growth Des.*, 3 (2003) 13–16.
4) B. Ruiz, B. J. Coe, R. Gianotti, V. Gramlich, M. Jazbinseka and P. Gunter, Polymorphism, crystal growth and characterization of an organic nonlinear optical material: DAPSH, *CrystEngComm.*, 9 (2007) 772–776.

5) A. H. Reshak, S. Auluck, D. Stys, I. V. Kityk, H. Kamarudin, J. Berdowski and Z. Tylczynski, Dispersion of linear and non-linear optical susceptibilities for amino acid 2-aminopropanoic CH3CH(NH2)COOH single crystals: experimental and theoretical investigations, *J. Mater. Chem.*, 21 (2011) 17219–17228.

6) V. Murugesan, M. Saravanabhavan and M. Sekar, Synthesis, spectroscopic characterization and structural investigation of a new charge transfer complex of 2,6-diaminopyridine with 4-nitrophenylacetic acid: Antimicrobial, DNA binding/cleavage and antioxidant studies, *Spectrochim. Acta, Part A*, 147 (2015) 99–106.

7) A. Bhattacharyya, P. K. Bhaumik, A. Bauza, P. P. Jana, A. Frontera, M. G. B. Drewand S.Chattopadhyay, A combined experimental and computational study of supramolecular assemblies in ternary copper(II) complexes with a tetradentate N4 donor Schiff base and halides, *RSC Adv.*, 4 (2014) 58643-58651.

8) M. A. Spackman and D. Jayatilaka, Hirshfeld surface analysis, *CrystEngComm.*, 11 (2009) 19-32.

9) F. L. Hirshfeld, Bonded-atom fragments for describing molecular charge densities, *Theor. Chim. Acta*, 44 (1977) 129-138.

10) H. F. Clausen, M. S. Chevallier, M. A. Spackman and B. B. Iversen, Three new co-crystals of hydroquinone: crystal structures and Hirshfeld surface analysis of intermolecular interactions *New J. Chem.*, 34 (2010) 193-199.

11) M. A. Spackman and J. J. McKinnon, Fingerprinting intermolecular interactions in molecular crystals, *CrystEngComm.*, 4 (2002) 378-392.

12) P. De, M. Baltas and F. Bedos-Belval, Cinnamic acid derivatives as Anticancer Agents – A review, *Curr .Med. Chem.*, 2011, 18, 1672-1703.

13) G. K. Yoya, F. Bedos-Belval, P. Constant, H. Duran, M. Daffe and M. Baltas, Synthesis and evolution of a novel series of pseudo-cinnamic derivatives as antituberculosis agents, *Bioorg. Med. Chem. Lett*., 2009, 19, 341-343.

14) J. Wiesner, A. Mitsch, P. Wiβner, H. Jomaa and M. Schliter, Structure–activity relationships of novel anti-malarial agents. Part 2: cinnamic acid derivatives, *Bioorg. Med. Chem. Lett*., 2001, 11, 423-424.

15) S. Tawata, S. Taira, N. Kobamoto, J. Zhu, M. Ishihara and S. Toyama, Synthesis and Antifungal Activity of Cinnamic Acid Esters, *Biosci. Biotechnol. Biochem*., 1996, 60, 909-910.

16) M. Soya, Antioxidant and Antimicrobial Activities of Cinnamic Acid Derivatives, *Mini Rev. Med. Chem*., 2012, 12, 749-767.

17) W. Nong, Z. Anran, J. Wei, X. Lin, L. Wang and C. Lin, Synthesis and biological evaluation of a new series of cinnamic acid amide derivatives as potent haemostatic agents containing a 2-aminothiazole substructure, *Bioorg. Med. Chem. Lett*., 2017, 27, 4506-4511.

18) S. Alen, D. Sajan, K. Job Sabu, K. Udaya Lakshmi, V. Veeraiah, K. Chaitanya and V. Bena Jothy, Studies on crystal growth, vibrational, dielectric, electronic, mechanical and thermal properties of new organic nonlinear optical crystal: 3-nitrocinnamic acid, *CrystEngComm*., 15 (2013) 9176-9188.

19) P. Balamurugaraj, S. Suresh, P. Koteeswari and P. Mani, Growth, Optical, Mechanical, Dielectric and Photoconductivity Properties of L-Proline Succinate NLO Single Crystal, Journal of Materials Physics and Chemistry., 1, (2013) 4-8.

20) K. M. Athira and K. Naseema, Non-linear optical studies of a new amino compound L-hydroxyproline picrate, *Indian J. Sci. Res.*, 18 (2018) 37-40.

21) C. A. G. N. Montalbetti and V. Falque, Amide bond formation and peptide couling, *Tetrahedron.*, 61 (2005) 10827 – 10852.

22) A. Leggio, E. L. Belsito, G. De Luca, M. L. Di Gioia, V. Leotta, E. Romio, C. Siciliano and A. Liguori, One-pot synthesis of amides from carboxylic acids activated using thionyl chloride, *RSC Adv.*, 6 (2016) 34468-34475.

23) G. G. Tu, S. H. Li, H. M. Huang, G. Li, F. Xiong, X. Mai, H. W. Zhu, B. H. Kuang and W. F. Xu, Novel aminopeptidase N inhibitors derived from 1,3,4-thiadiazole scaffold, *Bioorg. Med. Chem.*, 16 (2008) 6663 – 6668.

24) R.W.F. Bader, Atoms in Molecules: A Quantum Theory, Oxford University Press, Oxford, UK, 1990.

25) E.R. Johnson, S. Keinan, P. Mori-Sanchez, J. Contreras-Garcia, A.J. Cohen and W.J. Yang, Revealing Noncovalent Interactions, *J.Am.Chem.Soc.*, 132 (2010) 6498-6506.

26) I. Cukrowski, J.H. de Lange, A.S. Adeyinka and P. Mangondo, Evaluating common QTAIM and NCI interpretations of the electron density concentration through IQA interaction energies and 1D cross-sections of the electron and deformation density distributions Computational and Theoretical Chemistry, 1053 (2015) 60-76.

27) G. M. Sheldrick, SHELXTL Version 2014/7.
http://shelx.uni-ac.gwdg.de/SHELX/index.php

28) G. M. Sheldrick, A short history of SHELX, *Acta Cryst. A.*, 64 (2008) 112–122.

29) H. D. Flack, G. Bernardinelli, Absolute structure and absolute configuration, *Acta Cryst. A.*, 55 (1999) 908–915.

30) A. L. Spek, Structure validation in chemical crystallography, *Acta Cryst. D.*, 65 (2009) 148-155.

31) L. J. Farrugia, ORTEP-3 for Windows - a version of ORTEP-III with a Graphical User Interface (GUI), *J. Appl. Cryst.*, 30 (1997) 565.

32) C. F. Macrae, I. J. Bruno, J. A. Chisholm, P. R. Edgington, P. McCabe, E. Pidcock, L. Rodriguez-Monge, R. Taylor, J. van de Streek and P. A. Wood, Mercury CSD 2.0 - new features for the visualization and investigation of crystal structures, *J. Appl. Cryst.*, 41 (2008) 466-470.

33) M. Nardelli, PARST95 - an update to PARST: a system of Fortran routines for calculating molecular structure parameters from the results of crystal structure analyses, *J. Appl. Cryst.*, 28 (1995) 659.

34) F. Neese, The ORCA program system *Wiley Interdiscip. Rev.: Comput. Mol. Sci..*, 2 (2012) 73-78.

35) K. Aidas, C. Angeli, K. L. Bak, V. Bakken, R. Bast, L. Boman, O. Christiansen, R. Cimiraglia, S. Coriani, P. Dahle, E. K. Dalskov, U. Ekstroem, T. Enevoldsen, J. J. Eriksen, P. Ettenhuber, B. Fernandez, L. Ferrighi, H. Fliegl, L. Frediani, K. Hald, A. Halkier, C. Haettig, H. Heiberg, T. Helgaker, A. C. Hennum, H. Hettema, E. Hjertenaes, S. Hoest, I.-M. Hoeyvik, M. F. Iozzi, B. Jansik, H. J. Aa. Jensen, D. Jonsson, P. Joergensen, J. Kauczor, S. Kirpekar, T. Kjaergaard, W. Klopper, S. Knecht, R. Kobayashi, H. Koch, J. Kongsted, A. Krapp, K. Kristensen, A. Ligabue, O. B. Lutnaes, J. I. Melo, K. V. Mikkelsen, R. H. Myhre, C. Neiss, C. B. Nielsen, P. Norman, J. Olsen, J. M. H. Olsen, A. Osted, M. J. Packer, F. Pawlowski, T. B. Pedersen, P. F. Provasi, S. Reine, Z. Rinkevicius, T. A. Ruden, K. Ruud, V. Rybkin, P. Salek, C. C. M. Samson, A.

Sanchez de Meras, T. Saue, S. P. A. Sauer, B. Schimmelpfennig, K. Sneskov, A. H. Steindal, K. O. Sylvester-Hvid, P. R. Taylor, A. M. Teale, E. I. Tellgren, D. P. Tew, A. J. Thorvaldsen, L. Thoegersen, O. Vahtras, M. A. Watson, D. J. D. Wilson, M. Ziolkowski, H. Agren, "The Dalton quantum chemistry program system", *WIREs Comput. Mol. Sci*., 4 (2014) 269-284. (doi:10.1002/wcms.1172)

36) Dalton, a Molecular Electronic Structure Program,Release Dalton2016.2 (2016), see http://daltonprogram.org

37) M.J. Frisch, J.A. Pople and J.S. Binkley, Self-consistent molecular orbital methods 25. Supplementary functions for Gaussian basis sets, *J. Chem. Phys.*, 80 (1984) 3265.

38) T. Yanai, D. P. Tew and N.C. Handy, A new hybrid exchange–correlation functional using the Coulomb-attenuating method (CAM-B3LYP), *Chem. Phys. Lett.*, 393 (2004) 51–57.

39) D. Paschoal, HF Dos Santos, Assessing the quantum mechanical level of theory for prediction of linear and nonlinear optical properties of push-pull organic molecules, *J. Mol. Model.*, 19 (2013) 2079–2090.

40) A. K. S. M. Valdo, C. C. da Silva, L. J. Q. Maia, A. M. Sarotti and F. T. Martins, Experimental and theoretical second harmonic generation and photoluminescence from the pseudo-centrosymmetric dihydrochloride salt dihydrate of trans-1,2-bis(4-pyridyl)ethane, *CrystEngComm.*, 19 (2017) 346-354.

41) T. Lu and F. Chen, MULTIWFN: A Multifunctional wavefunction analyzer, *J. Comp. Chem.*, 33 (2012) 580-592.

42) J. Contreras-García, E.R. Johnson, S. Keinan, R. Chaudret, J.-P. Piquemal, D.N.Beratan and W. Yang, NCIPLOT: A Program for Plotting Non covalent Interaction Regions, *J. Chem. Theor. Comp.*, 7 (2011) 625-632.

43) W. Humpherey, A. Dalke and K. Schulten, VMD: Visual molecular dynamics, *J. Mol. Graph.*, 14 (1996) 33-38.

44) T. Ashida and M. Kakudo, Conformations of Prolyl Residues in Oligopeptides, *Bull. Chem. Soc. Jpn.*, 47 (1974) 1129-1133.

45) M. E. Kamwaya, O. Oster, H. Bradaczek, M. N. Ponnuswamy, S. Parthasarathy, R. Nagaraj and P. Balaram, Structure of tert-butyloxycarbonyl-L-alanyl-L-proline monohydrate (t-Boc-Ala-Pro), *Acta Cryst. B.*, 38 (1982) 172-176.

46) D. Cremer and J.A. Pople, General definition of ring puckering coordinates *J. Amer. Chem. Soc.*, 97 (1975) 1354-1358.

47) (i) K. Rajagopal, R.V. Krishnakumar, A. Mostad and S. Natarajan, L-Prolinium trichloroacetate at 105 K, *Acta Cryst. E.*, 59 (2003) o277–o279.

(ii) D. Ajo, V. Busetti and G. Granozzi, Conformational flexibility of dehydroalanine derivatives. Crystal and molecular structure of 2-n-acetyldehydrophenylalanyl-l-proline, *Tetrahedron*., 38 (1982) 3329 -3334.

48) J. Suresh, M. Venkateshan, S. Ponnuchamy, R. R. Kumar and P. L N. Lakshman, 3-[2-Cyclo-propyl-1-(2-fluoro-phenyl)-2-oxoethyl]-5-(4-methyl-sulfanyl-benzylidene)-1,3-thiazolidine-2,4-dione *Acta. Cryst. E*., 69 (2013) o188.

49) J. J. McKinnon, A. S. Mitchell and M. A. Spackman, Hirshfeld Surfaces: A New Tool for Visualising and Exploring Molecular Crystals, *Chem. Eur. J.*, 4 (1998) 2136-2141.

50) S. K. Wolff, D. J. Grimwood, J. J. McKinnon, M. J. Turner, D. Jayatilaka and M. A. Spackman, CrystalExplorer (Version 3.1), University of Western Australia., 2012.

51) A. Y. Meyer, The size of molecules, *Chem. Soc. Rev.*, 15 (1986) 449-474.

52) A. Baumgartner, Shapes of flexible vesicles at constant volume, *J. Chem. Phys.*, 98 (1993) 7496-7501.

53) R. S. Rowland and R. Taylor, Intermolecular Nonbonded Contact Distances in Organic Crystal Structures: Comparison with Distances Expected from van der Waals Radii, *J. Phys. Chem.*, 100 (1996) 7384-7391.

54) A. Bondi, van der Waals Volumes and Radii, *J. Phys. Chem.*, 68 (1964) 441-451.

55) B. Babu, J. Chandrasekaran, B. Mohanbabu, Y. Matsushita and M. Saravanakumar, Growth, physicochemical and quantum chemical investigations on 2-amino 5-chloropyridinium 4-carboxybutanoate – an organic crystal for biological and optoelectronic device applications, *RSC Adv.*, 6 (2016) 110884-110897.

56) J. J. McKinnon, D. Jayatilaka and M. A. Spackman, Towards quantitative analysis of intermolecular interactions with Hirshfeld surfaces, *Chem. Commun*., 0 (2007) 3814-3816.

57) P. L. A. Popelier, Characterization of a Dihydrogen Bond on the Basis of the Electron Density, *J. Phys. Chem. A.*, 102 (1998), 1873-1878.

58) M. Chahkandi, M. H. Bhatti, U. Yunus, S. Shaheen, M. Nadeem and M. N. Tahir, Synthesis and comprehensive structural studies of a novel amide based carboxylic acid derivative: Non-covalent interactions, *J. Mol. Struct*., 1133 (2017) 499-509.

59) J. Hernandez-Paredes, R. C. Carrillo-Torres, O. Hernandz-Negrete, R. R. Sotelo-Mundo, D. Glossman-Mitnik, H. E. Esparza-Ponce and M. E. Alvarez-Ramos, Experimental and

theoretical study on the molecular structure, covalent and non-covalent interactions of 2,4-dinitrodiphenylamine: X-ray diffraction and QTAIM approach, *J. Mol. Struct*., 1141 (2017) 53-63.

60) C. A. Mebi, DFT study on structure, electronic properties, and reactivity of cis-isomers of $[(NC_5H_4\text{-}S)_2Fe(CO)_2]$, *J. Chem. Sci.*, 123 (2011) 727-731.

61) V. Sivasubramani, V. Mohankumar, M. Senthil Pandian and P. Ramasamy, Synthesis, crystal growth, physicochemical properties and quantum chemical investigations of a D–π–A type organic single crystal: 2-amino-5-nitropyridinium p-phenolsulfonate (2A5NPP) for nonlinear optical (NLO) applications, *CrystEngComm*., 19 (2017) 5662-5678.

62) R. H. Abu-Eittah, M. K. Khedr, M. Goma and W. Zordok, The structure of Cinnamic acid and Cinnamoyl azides, a unique localized π system: The electronic spectra and DFT-treatment, Int. J. Quant. Chem., 112 (2012)1256-1272.

63) S. K. Kurtz and T. T. Perry, A Powder Technique for the Evaluation of Nonlinear Optical Materials, *J. Appl. Phys.*, 39 (1968) 3798–3815.

64) A. Dennis Raj, M. Jeeva, M. Shankar, R. Purusothaman, G. Venkatesa Prabhu and I. Vetha Potheher, Synthesis, growth, optical and DFT calculation of 2-naphthol derived Mannich base organic non linear optical single crystal for frequency conversion applications, *Physica B: Condens. Matter.*, 501 (2016) 45-56.

65) W. Wu, D. Wu, W. Cheng, H. Zhang and J. Dai, Syntheses, Crystal Growths, and Nonlinear Optical Properties for 2-Carboxylic acid-4-nitropyridine-1-oxide Crystals with Two Different Arrangements of Chromophores, *Cryst. Growth Des.*, 7 (2007) 2316-2323.

66) T. Chen, Z. Sun, X. Liu, J. Wang, Y. Zhou, C. Ji, S. Zhang, L. Li, Z. N. Chen and J. Luo, Strong enhancement of second harmonic generation in nonlinear optical crystals: 2-amino-3-nitropyridinium halides (Cl, Br, I), *J. Mater. Chem. C.*, 2 (2014) 8723-8728.

Table caption

Table 1: SXRD crystallographic data of CP.

Table 2: Conformation angles of Pyrrolidine ring.

Table 3: Hydrogen bonds of CP from PARST [Å and °].

Table 4: QTAIM descriptors of the BCPs for the intermolecular interactions present in the structure.

Table 5: FTIR vibrational frequencies assignment.

Table 6: Calculated dipole moment, polarizability, first-order hyperpolarizabilities (β) and second-order susceptibility $\chi^{(2)}$.

Table 1: SXRD crystallographic data of CP.

Empirical formula	C_{14} H_{15} N O_3
Formula weight	245.27
Temperature	293(2) K
Wavelength	0.71073 Å
Crystal system	Trigonal
Space group	P 31
Unit cell dimensions	a = 15.9976(10) Å;
	b = 15.9976(10) Å;
	c = 13.4251(7) Å;
Volume	2975.5(4) $Å^3$
Z	9
Density (calculated)	1.232 Mg/m^3
Absorption coefficient	0.087 mm^{-1}
F(000)	1170
Crystal size	0.21 x 0.20 x 0.18 mm^3
Theta range for data collection	1.470 to 25.350°.
Index ranges	-19<=h<=19, -19<=k<=19, -16<=l<=16
Reflections collected	36504
Independent reflections	7262 [R(int) = 0.0745]
Completeness to theta = 25.242°	100.0 %
Max. and min. transmission	0.974 and 0.967
Data / restraints / parameters	7262 / 1 / 489
Goodness-of-fit on F^2	1.001
Final R indices [I>2sigma(I)]	R1 = 0.0464, wR2 = 0.0880
R indices (all data)	R1 = 0.1309, wR2 = 0.1140
Absolute structure parameter	-0.1(15)
Extinction coefficient	0.0028(6)
Largest diff. peak and hole	0.164 and -0.145 $e.Å^{-3}$

Table 2: Conformation angles of pyrrolidine ring.

Molecule	χ^1	χ^2	χ^3	χ^4	θ	q_2	φ_2
A	30.8(6)	-35.2(8)	24.9(8)	-4.6(7)	-16.5(6)°	0.334(8) (Å)	100.0(11)°
B	33.9(6)	-36.8(6)	25.1(6)	-3.0(6)	-19.4(6)°	0.360(7) (Å)	102.5(10)°
C	30.6(6)	-35.1(7)	25.1(7)	-5.6(7)	-15.2(6)°	0.333(7) (Å)	97.9(10)°

Table 3: Hydrogen bonds for CP from PARST [Å and °].

D-H...A	d(D-H)	d(H...A)	d(D...A)	<(DHA)
C1C -H1C ...O3A #0	0.93	2.486	3.403	168.81
C8C -H8C ...O3A #0	0.93	2.652	3.546	161.22
O2A -H2A1 ...O1A #1	0.82	1.827	2.606	158.03
C2C -H2C ...O1A #1	0.93	2.661	3.391	135.87
C2A -H2A ...O1B #2	0.93	2.891	3.474	121.98
C3A -H3A ...O2A #2	0.93	2.837	3.493	128.54
C3B -H3B ...O2B #2	0.93	2.847	3.499	128.25
C1A -H1A ...O1B #2	0.93	2.871	3.459	122.38
C2A -H2A ...O3B #3	0.93	2.472	3.333	154.06
C5A -H5A ...O2A #4	0.93	2.659	3.306	127.29
C4A -H4A ...O1A #4	0.93	2.838	3.687	152.34
C5A -H5A ...O1A #5	0.93	2.844	3.722	158.02
C7A -H7A ...O3A #5	0.93	2.660	3.343	130.76
O2B -H2B1 ...O1B #6	0.82	1.807	2.596	161.01
C2B -H2B ...O1C #6	0.93	2.715	3.404	131.60
C10B -H10D ...O3C #7	0.97	2.604	3.306	129.43
C1B -H1B ...O3C #7	0.93	2.667	3.578	166.43
C8B -H8B ...O3C #7	0.93	2.448	3.355	165.09
C5B -H5B ...O2B #8	0.93	2.670	3.308	126.46
C4B -H4B ...O1B #8	0.93	2.856	3.685	149.06
C7B -H7B ...O3B #9	0.93	2.630	3.319	131.35
C5B -H5B ...O1B #9	0.93	2.898	3.792	161.44
O2C -H2C1 ...O1C #10	0.82	1.835	2.617	159.04
C5C -H5C ...O2C #11	0.93	2.616	3.298	130.63
C4C -H4C ...O1C #11	0.93	2.819	3.673	153.17
C5C -H5C ...O1C #12	0.93	2.866	3.695	149.03

Symmetry transformations used to generate equivalent atoms:

#0 x,y,z; #1 -x+y,-x,+z-1/3; #2 x,+y,+z+1; # 3 -y+1,+x-y+1,+z+1/3+1

#4 -x+y,-x,+z+2/3; #5 -y,+x-y,+z+1/3; #6 -x+y,-x+1,+z-1/3;#7 -y,+x-y,+z-2/3

#8 -x+y,-x+1,+z+2/3; #9 -y+1,+x-y+1,+z+1/3; #10 -y+1,+x-y,+z+1/3;

#11 -y+1,+x-y,+z-2/3; #12 -x+y+1,-x+1,+z-1/3

Table 4: QTAIM descriptors of the BCPs for the intermolecular interactions present in the structure.

Interaction	ρ	$\nabla^2\rho$	G(r) a.u	V (r) a.u	H(r) a.u	$\frac{\lvert V(r)\rvert}{G(r)}$	E_{bond} kJ.mol^{-1}
O2B -H2B1...O1B #6	0.02894	0.11025	0.02555	-0.02354	0.00205	0.9213	-31.81
O2A -H2A1...O1A #1	0.02794	0.10481	0.02442	-0.02265	0.00177	0.9275	-30.608
O2C -H2C ...O1C #10	0.02763	0.10131	0.02377	-0.02222	0.00155	0.9348	-30.027
C2A -H2A ...O3B #3	0.01013	0.02627	0.00628	-0.00599	0.00028	0.9538	-8.095
C1C -H1C ...O3A #0	0.00916	0.02811	0.0065	-0.00598	0.00052	0.92	-8.081
C8B -H8B ...O3C #7	0.00831	0.02803	0.00632	-0.00594	0.00068	0.9399	-8.027
C2A -H2A ...O1B #2	0.0086	0.02848	0.00605	-0.00561	0.00043	0.927	-7.581
C10B-H10D...O3C #7	0.00717	0.02367	0.00524	-0.00456	0.00067	0.8702	-6.162
C7B -H7B ...O3B #9	0.00719	0.02294	0.00507	-0.00441	0.00066	0.8698	-5.959
C2C -H2C ...O1A #1	0.0068	0.0215	0.00478	-0.00418	0.00059	0.8745	-5.648
C7A -H7A ...O3A #5	0.00681	0.02204	0.00484	-0.00417	0.00066	0.8616	-5.635
C5C -H5C ...O2C #11	0.00313	0.02224	0.00481	-0.00404	0.00076	0.84	-5.459
C5B -H5B ...O2B #8	0.0062	0.02161	0.00467	-0.00394	0.00073	0.8436	-5.324
C5A -H5A ...O2A #4	0.00602	0.02145	0.00461	-0.00385	0.00076	0.8351	-5.203
C5A -H5A ...O1A #5	0.00599	0.02149	0.00461	-0.00384	0.00076	0.8329	-5.189
C1B -H1B ...O3C #7	0.00615	0.0189	0.00428	-0.00384	0.00044	0.8972	-5.189
C2B -H2B ...O1C #6	0.00621	0.02017	0.00442	-0.00379	0.00063	0.8575	-5.123
C8C -H8C ...O3A #0	0.00547	0.01888	0.00415	-0.00359	0.00015	0.8651	-4.851
C5C -H5C ...O1C #12	0.00588	0.02013	0.00425	-0.00348	0.00077	0.8188	-4.702
C1A -H1A ...O1B #2	0.00477	0.01683	0.00351	-0.00281	0.00069	0.8001	-3.797
C3A -H3A ...O2A #2	0.00221	0.01532	0.00324	-0.00266	0.00058	0.8209	-3.594
C3B -H3B ...O2B #2	0.0044	0.01521	0.00321	-0.00261	0.00059	0.8131	-3.527
C4A -H4A ...O1A #4	0.00398	0.01316	0.00281	-0.00233	0.00048	0.8292	-3.179
C4C -H4C ...O1C #11	0.00389	0.01305	0.00277	-0.00227	0.00049	0.8195	-3.065

C4B -H4B ...O1B #8	0.00351	0.01281	0.00269	-0.00217	0.00052	0.8067	-2.9324
C5B -H5B ...O1B #9	0.0031	0.01118	0.00232	-0.00184	0.00047	0.7931	-2.486

Symmetry transformations used to generate equivalent atoms:
#0 x,y,z; #1 -x+y,-x,+z-1/3; #2 x,+y,+z+1; #3 -y+1,+x-y+1,+z+1/3+1;
#4 -x+y,-x,+z+2/3; #5 -y,+x-y,+z+1/3; #6 -x+y,-x+1,+z-1/3;#7 -y,+x-y,+z-2/3;
#8 -x+y,-x+1,+z+2/3; #9 -y+1,+x-y+1,+z+1/3; #10 -y+1,+x-y,+z+1/3;
#11 -y+1,+x-y,+z-2/3; #12 -x+y+1,-x+1,+z-1/3

Table 5: FTIR vibrational frequencies assignment.

Experimental frequency (cm-1)	Theoretical frequency (cm-1)	Assignments
653	651	C-H bending
767	757	C-H out of plane bending
	891	OH…O out of plane wagging
902	902	Aryl C-H wagging
977	983	C-H out of plane deformation
	1171	C-O stretching
1193	1199	C-N stretching
1255	1249	C-N stretching
1323	1336	C-H in-plane deformation
	1381	C-OH in-plane bending
	1395	C-O stretching
1446	1497	Aryl C-C stretching
	1558	C-O stretching
1571	1587	C=O stretching
1647	1683	C=C skeletal vibration
1736	1745	C=O anti-symmetric stretching
3099	3097	C-H stretching
3194	3197	Aryl C-H stretching
3599	3591	O-H stretching

Table 6: Calculated dipole moment, polarizability, first-order hyperpolarizabilities β(x10^{-30} esu) and second-order susceptibility $\chi^{(2)}$.

Dipole moment	**Polarizability**[a]	**Hyper polarizability**[b]
μ_x -2.29007 a.u	α_{xx} 39.947	β_{XXX} -0.141
μ_y -1.15581 a.u	α_{yy} 25.255	β_{YYY} -0.31
μ_z 1.49565 a.u	α_{zz} 17.419	β_{ZZZ} -1.209
μ 2.96939 a.u	α_{xy} -6.012	β_{XYY} -0.025
μ 7.54759 D	α_{xz} -5.899	β_{XXY} -0.11
	α_{yz} 1.852	β_{XXZ} 0.045
	Δα 71.9583	β_{XZZ} -2.253
	α 27.54	β_{YZZ} 2.635
		β_{YYZ} 0.742
		β_{XYZ} -0.22
		β 3.307
		N = 0.336
		L = 1.1255
		$\chi^{(2)}$(cal) = 1.2506
		$\chi^{(2)}$(exp) = 3.456

[a] Unit for α is 10^{-24} esu.

[b] Unit for N is 10^{21} cm^{-3}, $\chi^{(2)}$ is 10^{-9} esu.

Figure caption

Fig. 1: Scheme of the reaction between Cinnamoyl chloride and L-proline with THF as a solvent.

Fig. 2: ORTEP diagram of CP with 50% probability.

Fig. 3: (a) O-H…O interaction viewed along the b axis, (b) Partial packing diagram viewed along c axis (Black - A molecule, Red – B molecule and Green – C molecule respectively).

Fig. 4: Experimental and simulated Powder X-ray diffraction patterns.

Fig. 5: Hirshfeld surface of CP with d_{norm} plotted from -0.757 (red) to 1.528 (blue) and its corresponding fingerprint plots of molecules A, B and C.

Fig. 6: Left: Colour coded NCI plot along with QTAIM CPs for molecules A, B and C. The small yellow spheres denote the CP's produced from QTAIM analysis. Right: 2D representation of NCI surface as sign(λ_2)ρ vs Reduced density gradient (S). (Colour coded as same as that of the NCI surface).

Fig. 7: Frontier molecular orbitals and energies of the HOMO, HOMO-1, HOMO-2, HOMO-3, HOMO-4, HOMO-5, HOMO-6, LUMO and LUMO+1 of CP.

Fig. 8: Theoretical and Observed UV-Vis spectrum of CP.

Fig. 9: Photoluminescence spectrum of CP.

Fig. 10: Experimental and theoretical IR spectra of CP.

Fig. 11: TG-DTA spectrum of CP.

Fig. 12: Comparison of powder SHG output of CP with KDP.

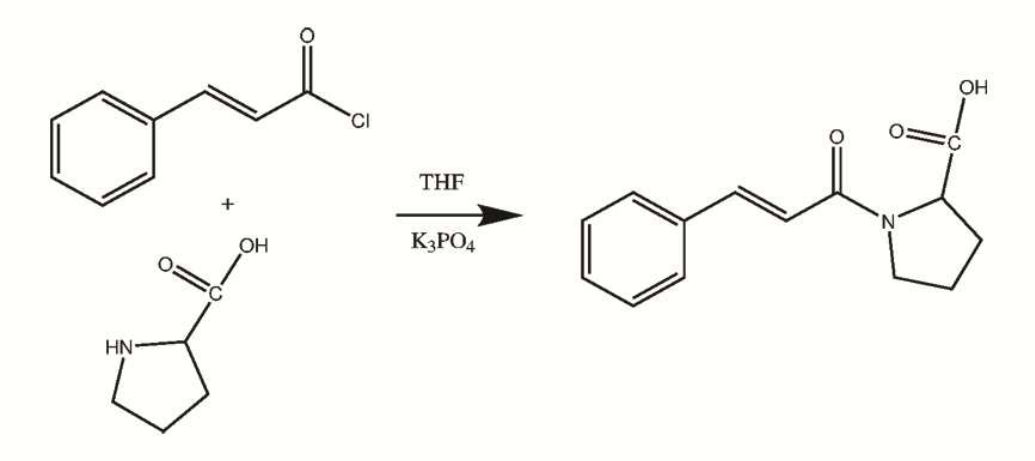

Fig. 1: Scheme of the reaction between Cinnamoyl chloride and L-proline with THF as a solvent.

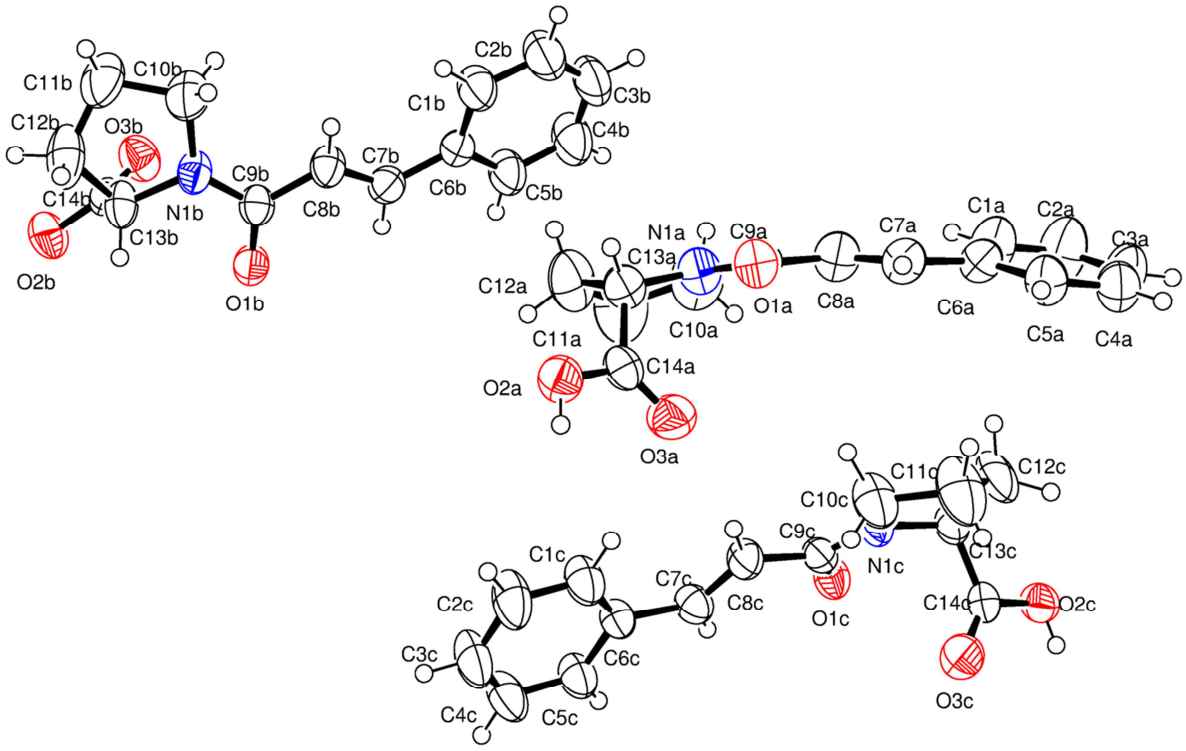

Fig. 2. ORTEP diagram of CP with 50% probability.

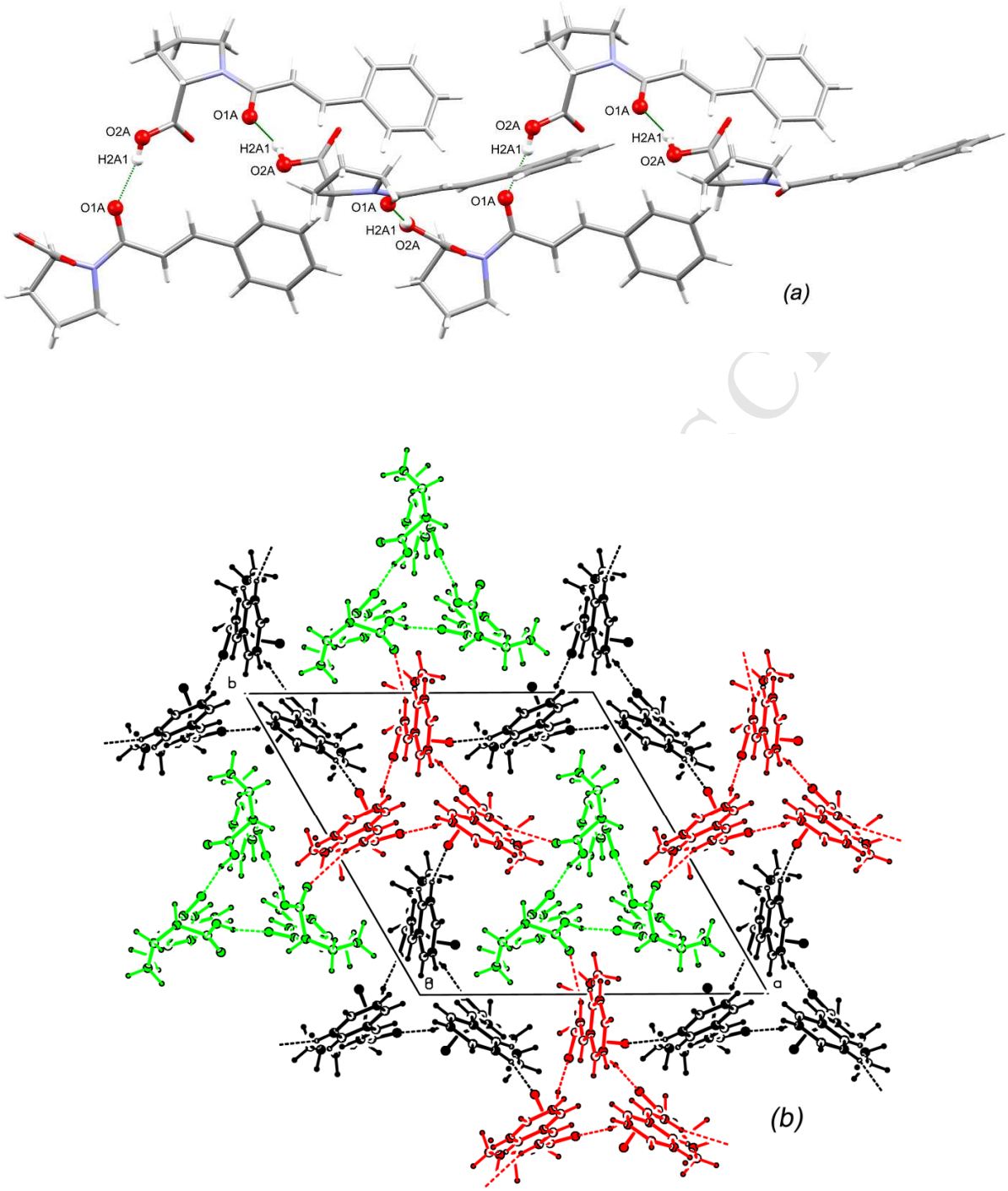

Fig. 3: (a) O-H…O interaction viewed along the b axis, (b) Partial packing diagram viewed along c axis (Black - A molecule, Red – B molecule and Green – C molecule respectively).

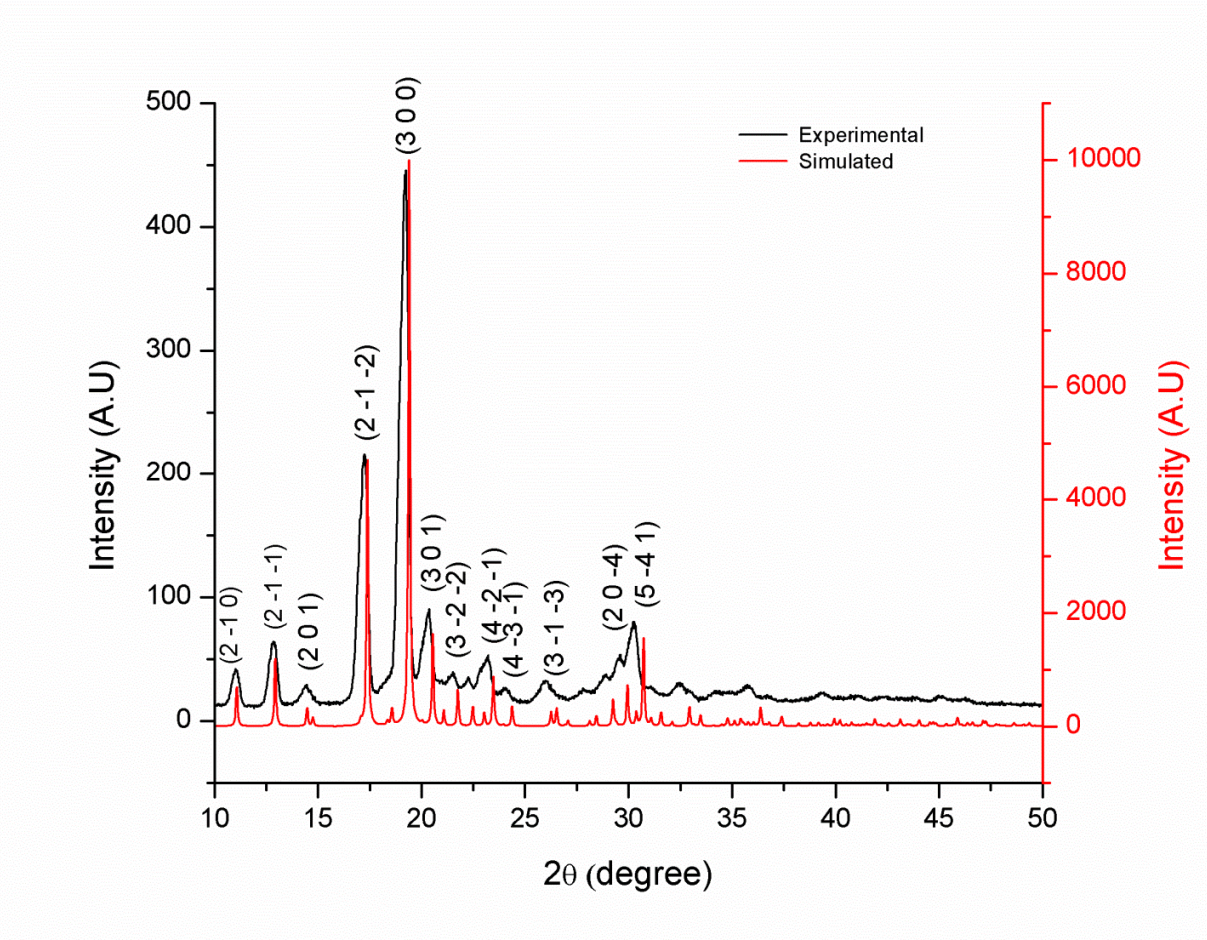

Fig. 4: Experimental and simulated Powder X-ray diffraction patterns.

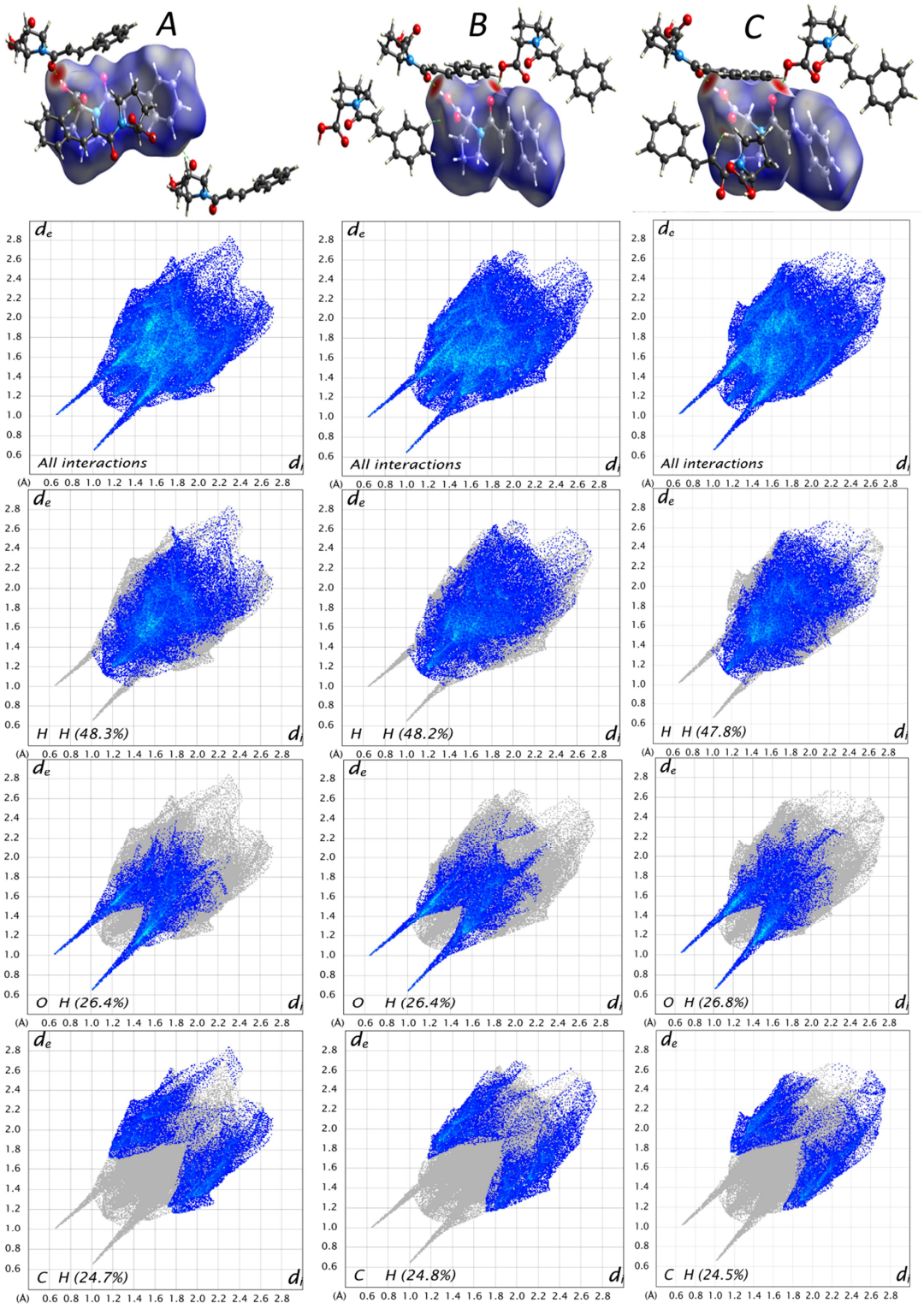

Fig. 5: Hirshfeld surface of CP with d_{norm} plotted from -0.757 (red) to 1.528 (blue) and its corresponding fingerprint plots of molecules A, B and C.

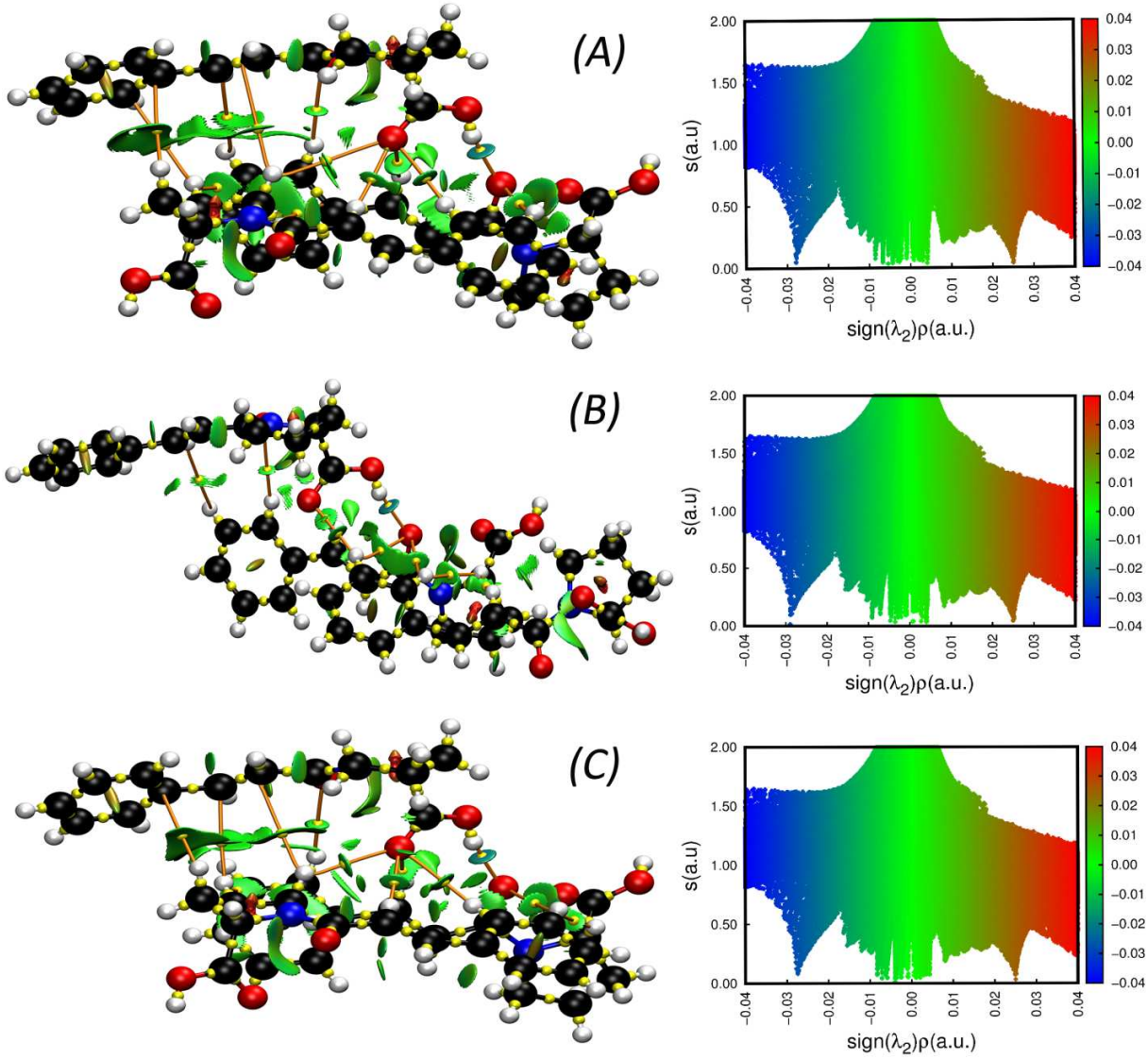

Fig. 6: Left: Colour coded NCI plot along with QTAIM CPs for molecules A, B and C. The small yellow spheres denote the CP's produced from QTAIM analysis. Right: 2D representation of NCI surface as sign(λ_2)ρ vs Reduced density gradient (S). (Colour coded as same as that of the NCI surface)

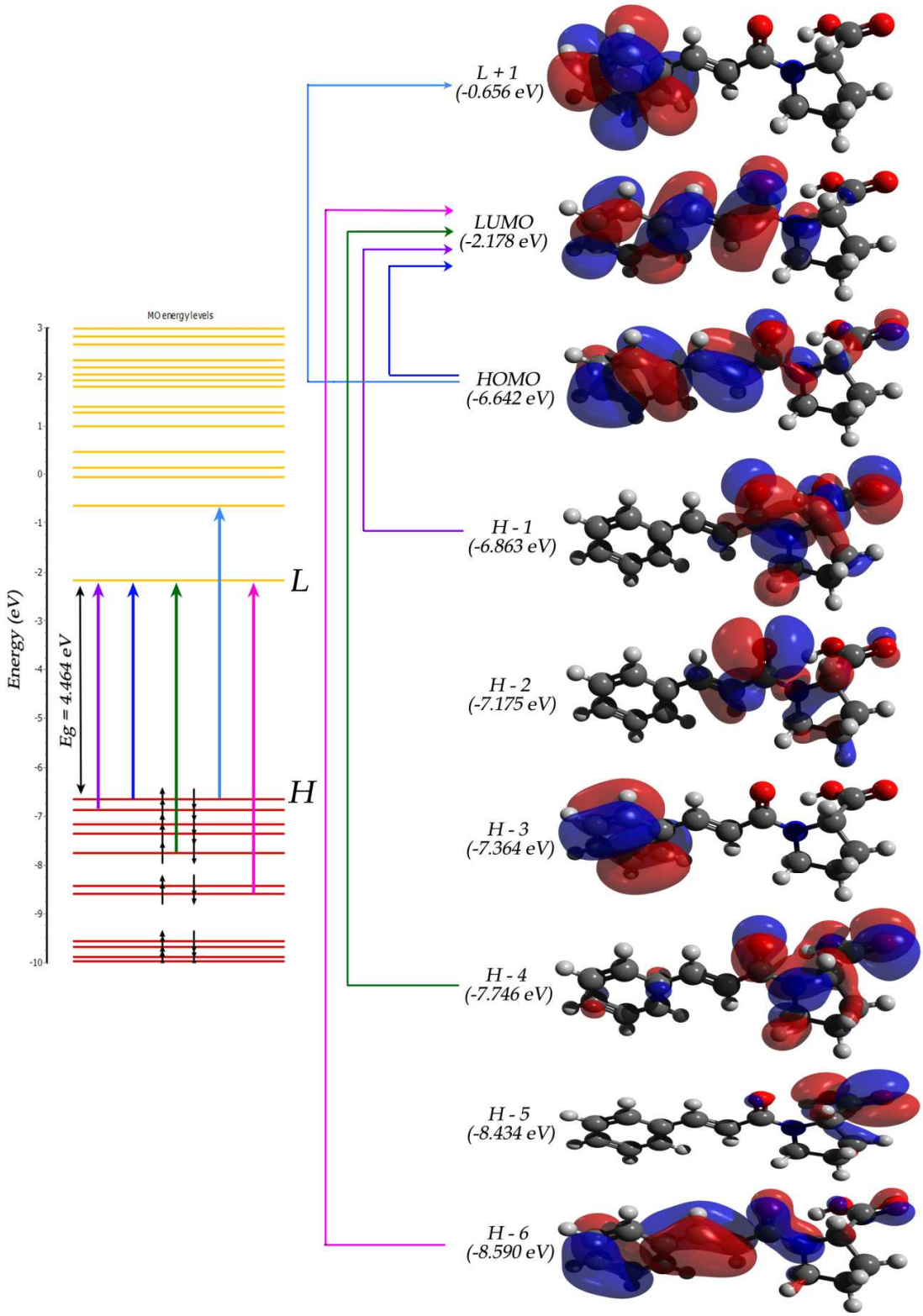

Fig. 7: Frontier molecular orbitals and energies of the HOMO, HOMO-1, HOMO-2, HOMO-3, HOMO-4, HOMO-5, HOMO-6, LUMO and LUMO+1 of CP.

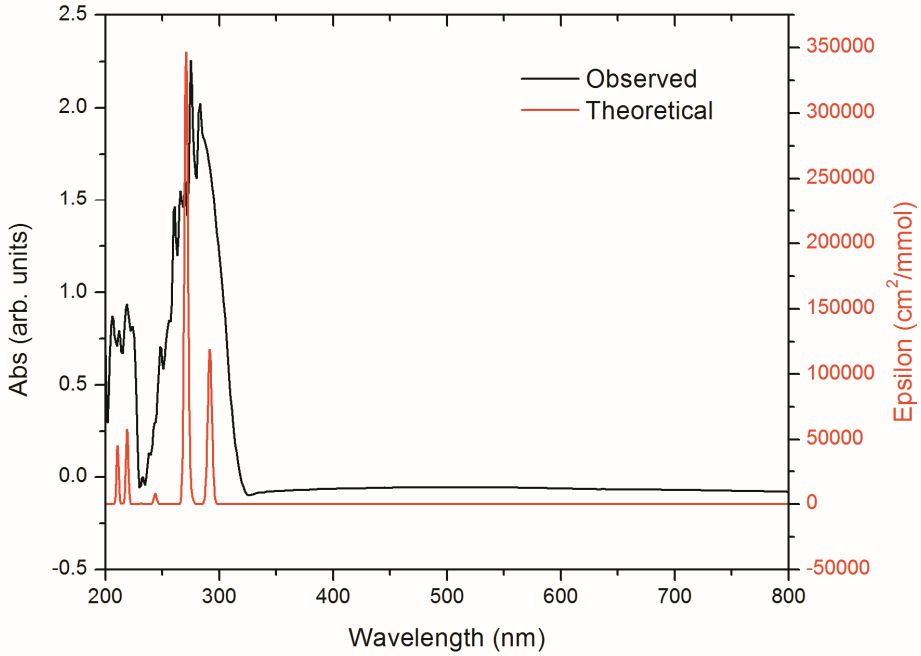

Fig. 8: Theoretical and Observed UV-Vis spectrum of CP.

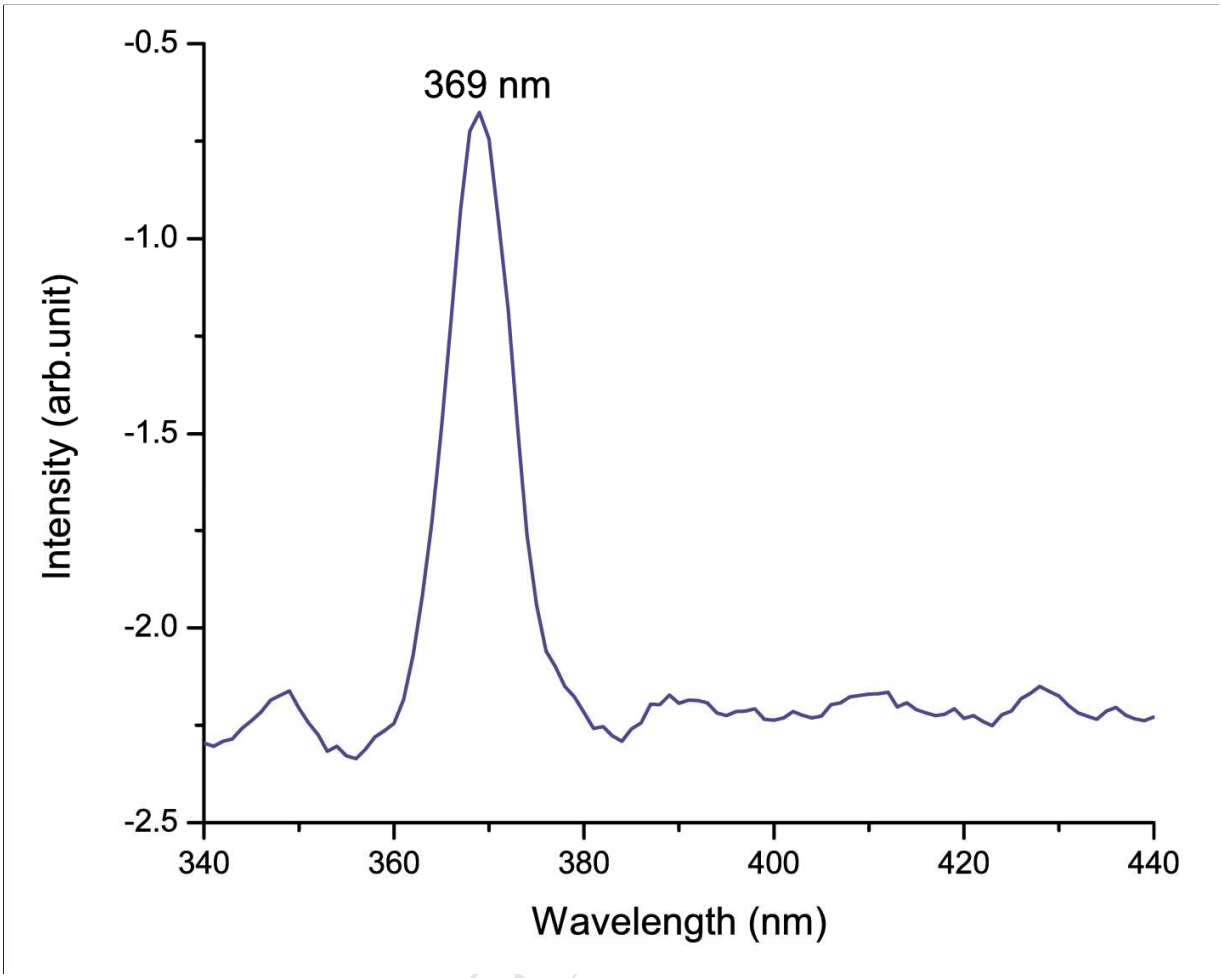

Fig. 9: Photoluminescence spectrum of CP.

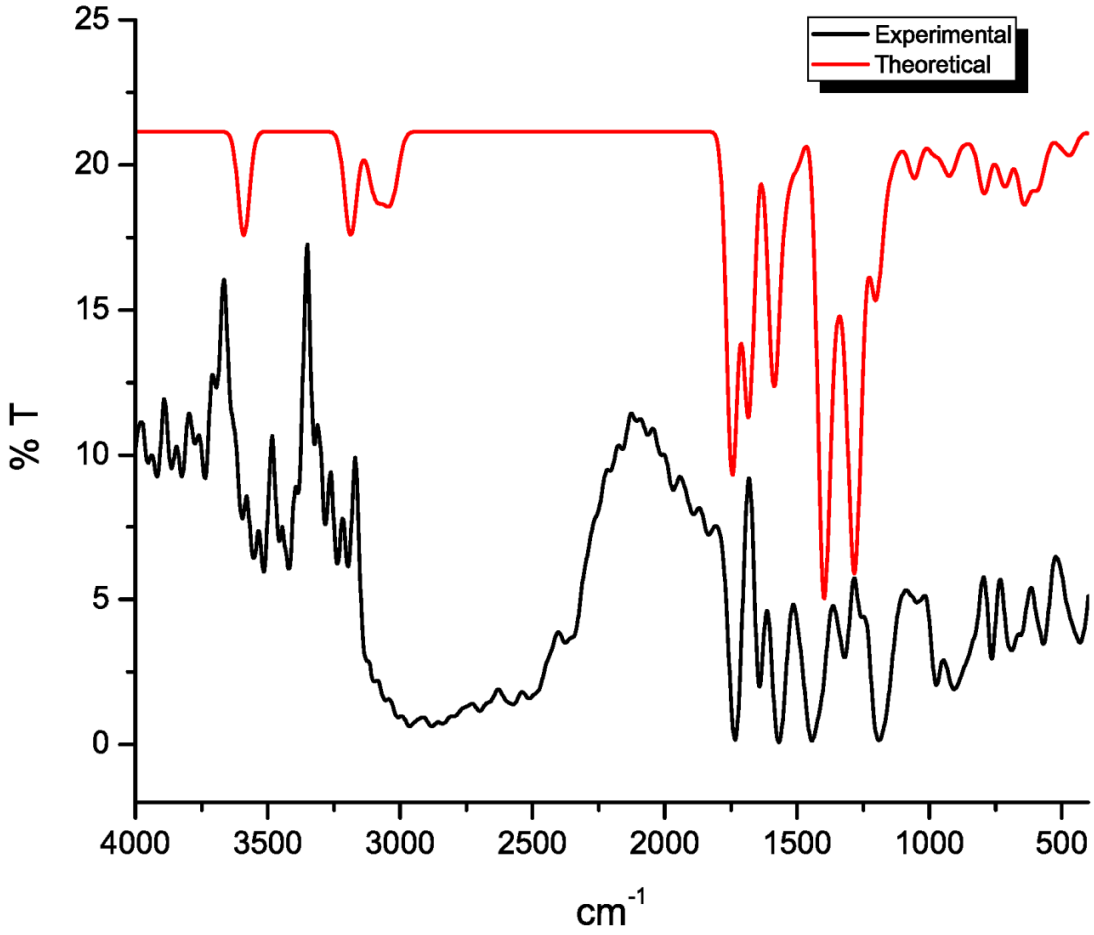

Fig. 10: FTIR spectrum of CP.

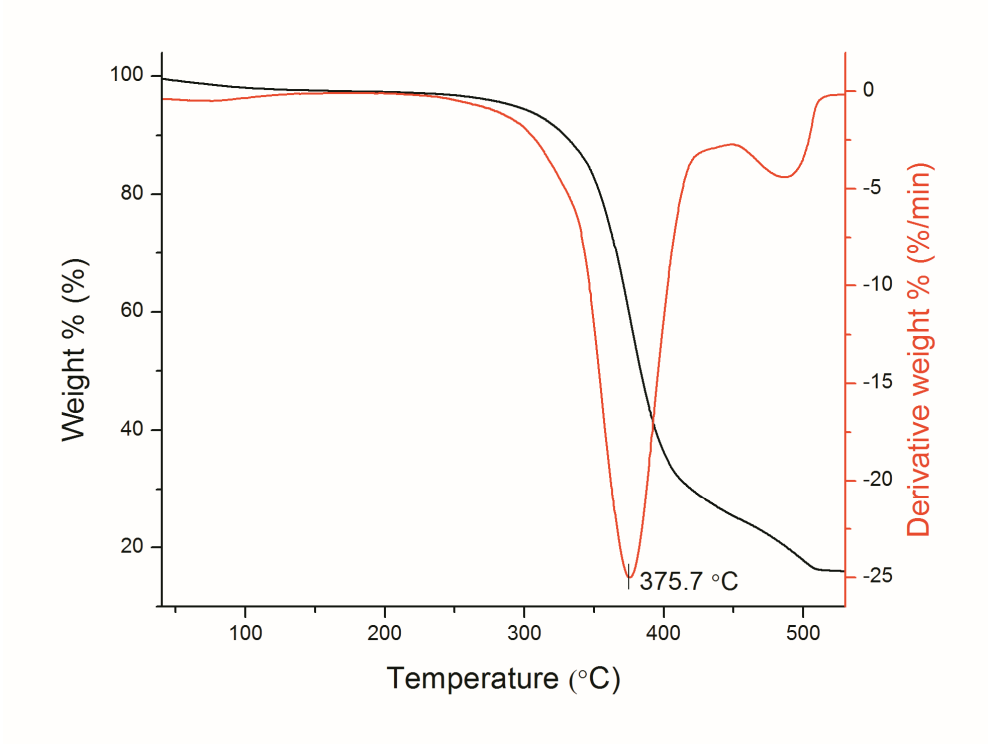

Fig. 11: TG-DTA spectrum of CP.

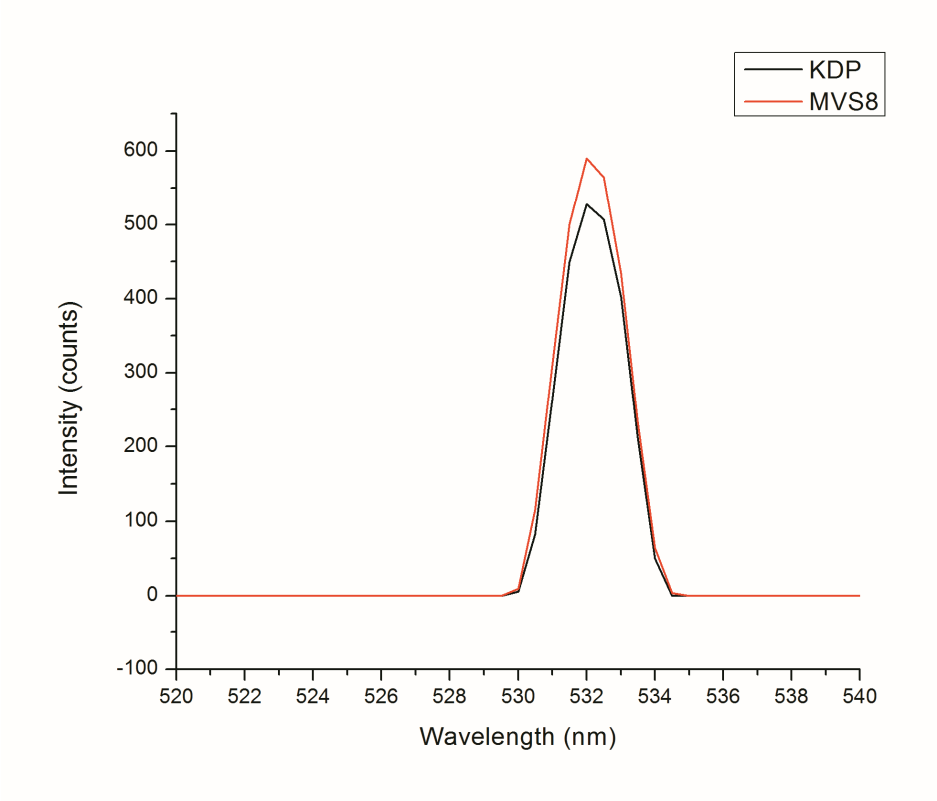

Fig. 12: Comparison of powder SHG output of CP with KDP.

Highlights:

- A new organic NLO material cinnamoylproline was synthesized and crystal was grown from solution technique.
- The material's intermolecular interactions were studied using Hirshfeld surface analysis.
- Topological properties were analyzed using QTAIM analysis. From which interaction energies were obtained. Non covalent interactions were visualized using NCIPLOT.
- NLO SHG efficiency was calculated from Kertz-perry powder method.
- Theoretical DFT analysis was done. Theoretical and experimental data were correlated. First hyperpolarizability and second order susceptibility was calculated and compared with the experimental results.